ACCOUNTS
of chemical research

A Theory for Bioinorganic Chemical Reactivity of Oxometal Complexes and Analogous Oxidants: The Exchange and Orbital-Selection Rules

DANDAMUDI USHARANI, DEEPA JANARDANAN, CHUNSEN LI, AND SASON SHAIK*

Institute of Chemistry and the Lise Meitner-Minerva Center for Computational Quantum Chemistry, The Hebrew University of Jerusalem, Givat Ram Campus, 91904 Jerusalem, Israel

RECEIVED ON JULY 12, 2012

CONSPECTUS

Over the past decades metalloenzymes and their synthetic models have emerged as an area of increasing research interest. The metalloenzymes and their synthetic models oxidize organic molecules using oxometal complexes (OMCs), especially oxoiron(IV)-based ones. Theoretical studies have helped researchers to characterize the active species and to resolve mechanistic issues. This activity has generated massive amounts of data on the relationship between the reactivity of OMCs and the transition metal's identity, oxidation state, ligand sphere, and spin state. Theoretical studies have also produced information on transition state (TS) structures, reaction intermediates, barriers, and rate–equilibrium relationships. For example, the experimental–theoretical interplay has revealed that nonheme enzymes carry out H-abstraction from strong C–H bonds using high-spin (S = 2) oxoiron(IV) species with four unpaired electrons on the iron center. However, other reagents with higher spin states and more unpaired electrons on the metal are not as reactive. Still other reagents carry out these transformations using lower spin states with fewer unpaired electrons on the metal. The TS structures for these reactions exhibit structural selectivity depending on the reactive spin states. The barriers and thermodynamic driving forces of the reactions also depend on the spin state. H-Abstraction is preferred over the thermodynamically more favorable concerted insertion into C–H bonds. Currently, there is no unified theoretical framework that explains the totality of these fascinating trends.

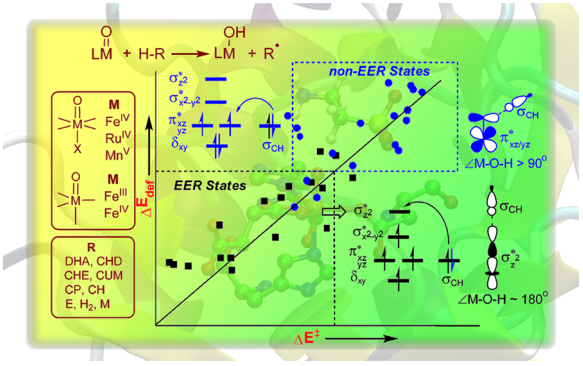

This Account aims to unify this rich chemistry and understand the role of unpaired electrons on chemical reactivity. We show that during an oxidative step the d-orbital block of the transition metal is enriched by one electron through proton-coupled electron transfer (PCET). That single electron elicits variable exchange interactions on the metal, which in turn depend critically on the number of unpaired electrons on the metal center. Thus, we introduce the exchange-enhanced reactivity (EER) principle, which predicts the preferred spin state during oxidation reactions, the dependence of the barrier on the number of unpaired electrons in the TS, and the dependence of the deformation energy of the reactants on the spin state. We complement EER with orbital-selection rules, which predict the structure of the preferred TS and provide a handy theory of bioinorganic oxidative reactions. These rules show how EER provides a Hund's Rule for chemical reactivity: EER controls the reactivity landscape for a great variety of transition-metal complexes and substrates. Among many reactivity patterns explained, EER rationalizes the abundance of high-spin oxoiron(IV) complexes in enzymes that carry out bond activation of the strongest bonds. The concepts used in this Account might also be applicable in other areas such as in f-block chemistry and excited-state reactivity of 4d and 5d OMCs.

Introduction

Nature uses oxoiron complexes in essential transformations[1] for metabolism of living organisms. For example, oxoiron(IV) moieties abound in heme enzymes,[1a] in α-ketoglutarate-dependent dioxygenases, such as, taurine:α-ketoglutarate dioxygenase (TauD), and pterin-dependent hydroxylases.[1b] Fe_2O_2 diamond cores function in hydroxylases and in desaturases.[1b,c] In Rieske dioxygenases,[1b] the implicated

Published on the Web 12/04/2012 www.pubs.acs.org/accounts
10.1021/ar300204y

species is oxo-hydroxoiron(V). In other enzymes, it is superoxoiron(III).[2] Scheme 1 shows transformations catalyzed by these species. Hydroxylation and desaturation, for example, are stepwise and are initiated by initial hydrogen atom transfer (HAT); others like oxygen-atom transfer (OAT) are concerted processes.

This richness, and the fact that nonheme enzymatic oxoiron(IV) species generally possess high-spin ground states, has propelled bioinorganic chemistry into creative design of high-valent oxometal complexes (OMCs) that can emulate or surpass Nature.[1,3] This activity has generated plenty of oxometal and nitridometal complexes,[3d,e] with different spin states and reactivity patterns. Computational chemistry has contributed essential insight into properties of these reactive intermediates and their mechanisms, thus leading to a fruitful experimental–theoretical interplay.[4] There comes a time for generalizations.

Our group has used density functional theory (DFT) to study such reactions.[5] Scheme 2a shows the complexes studied, arranged by ligand types. Scheme 2b depicts substrates used for reactivity investigations. This study has generated common insight, which is reviewed here with a focus on *the dominance of the spin-state identity* in shaping the reactivity landscape of these complexes.

In addition to factors that affect organic transformations, in bioinorganic reactions, the number of *unpaired electrons on the metal center* changes during the oxidation process, thereby creating *a highly variable exchange interaction* that favors some spin states and specific mechanisms as mediators of the transformation.[6–8] Furthermore, these favored states have transition states (TSs) with unique structural characteristics.[6–8] Accordingly, this Account articulates concepts that generalize these reactivity patterns. The first concept is the exchange-enhanced reactivity (EER),[6,9] which accounts for the high reactivity of certain spin states (e.g., S = 2 $Fe^{IV}O$ species) and for the ubiquity of stepwise over concerted mechanisms, for example, in C–H/C=C activation. Combining EER with orbital-selection rules[6b,c] leads to

SCHEME 1. Reactions of Oxoiron Complexes

$LFe^{IV}O$ $L_2Fe_2^{IV}O_2$ $LFe^{III}O_2^-$ $LFe^{V}O(OH)$

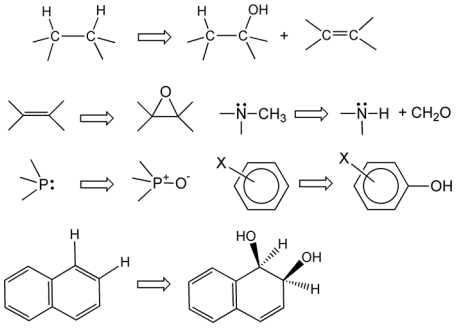

SCHEME 2. Oxidants (a) and Substrates (b) Studied by DFT[5]

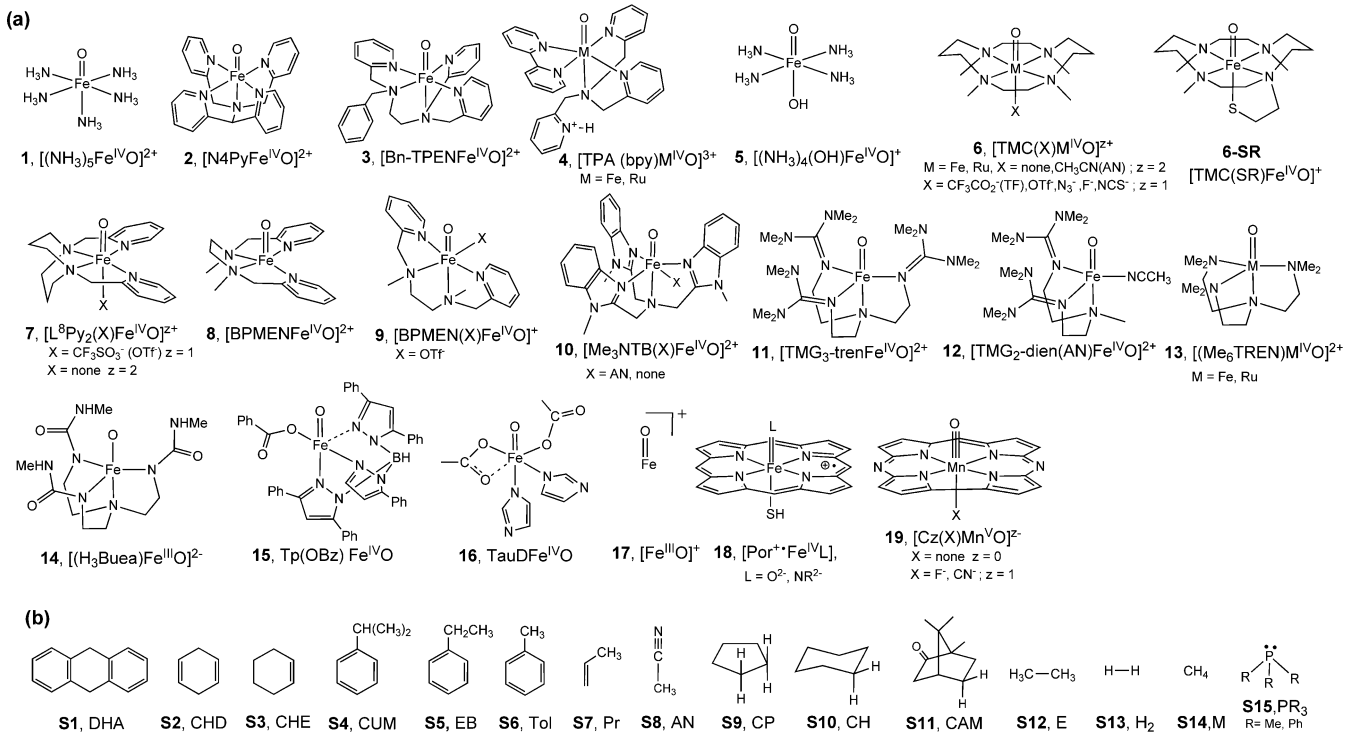

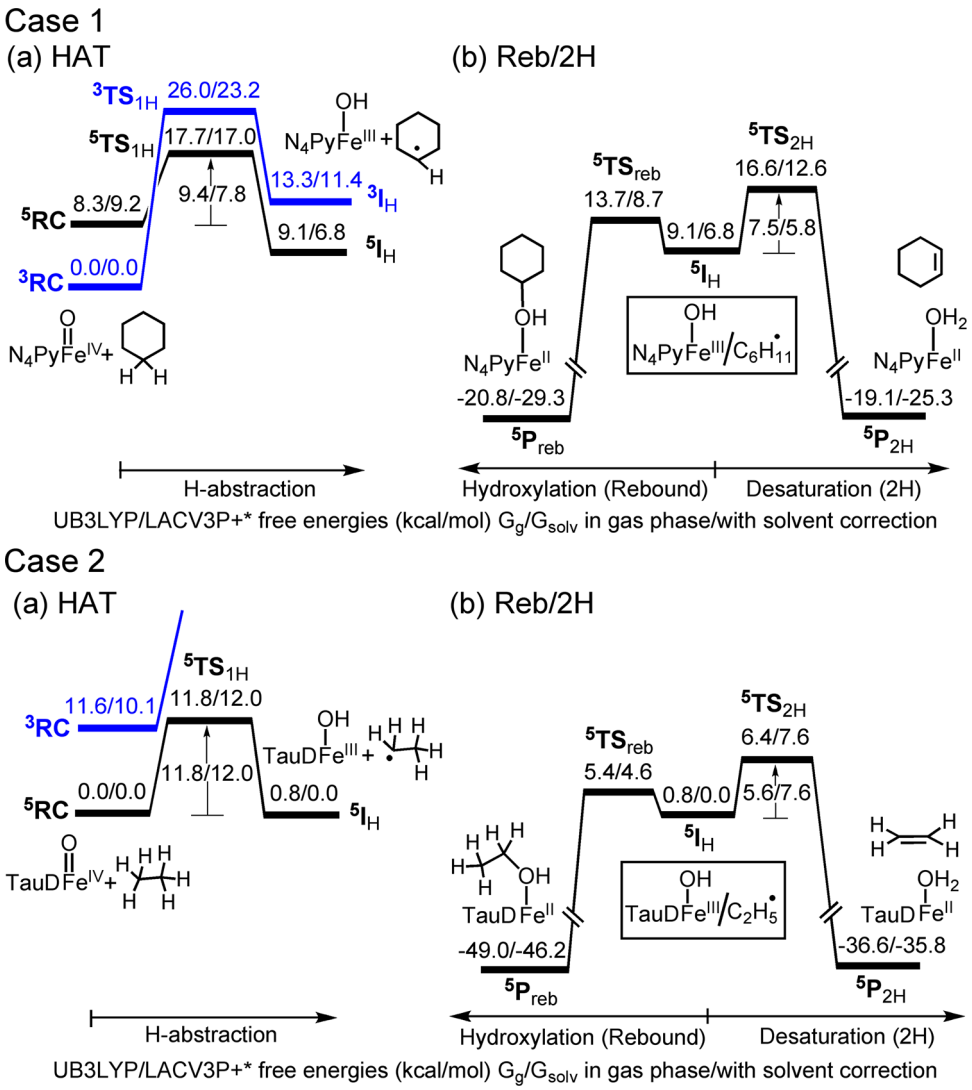

FIGURE 1. Alkane activation reaction profiles for oxidant/substrate pairs proceeding via HAT followed by rebound and/or desaturation (2H). Case 1: **2**/**S10**.[13] Case 2: **16**/**S12**.[5,15]

stereochemical predictions for the TSs in different spin states. Finally, the reactants' deformation energy in the TS[10] shows the origins of the EER effect on reaction barriers.

Alkane activation (Scheme 1) is a key reaction of OMCs; it commences with HAT and generates a variety of products. These mechanistic features are similar for other stepwise processes (e.g., epoxidation), and therefore, focusing on alkane activation will reveal general insight. Accordingly, we introduce first the EER concept,[9] using Fe^{IV}O HAT-reactivity, and subsequently, we outline the EER scope for other OMCs and oxidation reactions.

Alkane Activations by OMCs

Figure 1 shows archetypical cases of alkane activations representing the systems in Scheme 2, one describing two-state reactivity (TSR) and the other single-state reactivity.[11] Case 1 uses [N4PyFe^{IV}(O)]$^{2+}$ (**2**) as an octahedral example, with a strong-field ligand, reacting with cyclohexane (**S10**).[12] During HAT, in (a), the S = 1 ground state exhibits a high barrier, while the excited S = 2 state mediates the HAT with a low barrier, forming the ground state intermediate ^{5}I$_H$(Fe^{III}OH/R·).[6a,b,d,13] Subsequently, in (b), ^{5}I$_H$ bifurcates between rebound and desaturation. Since R· is weakly bound, it can also dissociate,[13] leading to a free radical that is trapped by O_2.[14] Case 2 typifies reactions of complexes with weak ligand fields, using for example the reaction of **16** with ethane (**S12**).[5,15] Here, S = 2 is the ground state that also mediates the HAT at a low barrier. S = 1 is higher lying.[4c,8b,16] Note the following: (i) The reactive state is S = 2 for both cases. (ii) The desaturation barrier nascent from Fe^{III}OH/R· is close to the first HAT *even though the thermodynamic driving force is much larger for desaturation*. The root cause of these

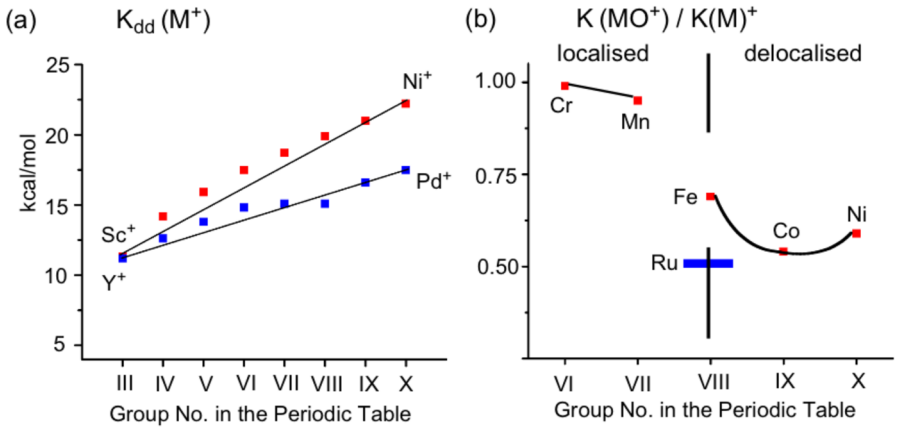

FIGURE 2. (a) K_{dd} values for transition-metal cations (M^+) in the 3d and 4d periods.[22,23] (b) Ratios of K_{dd} for OMCs (MO^+) to M^+.[9,22,23]

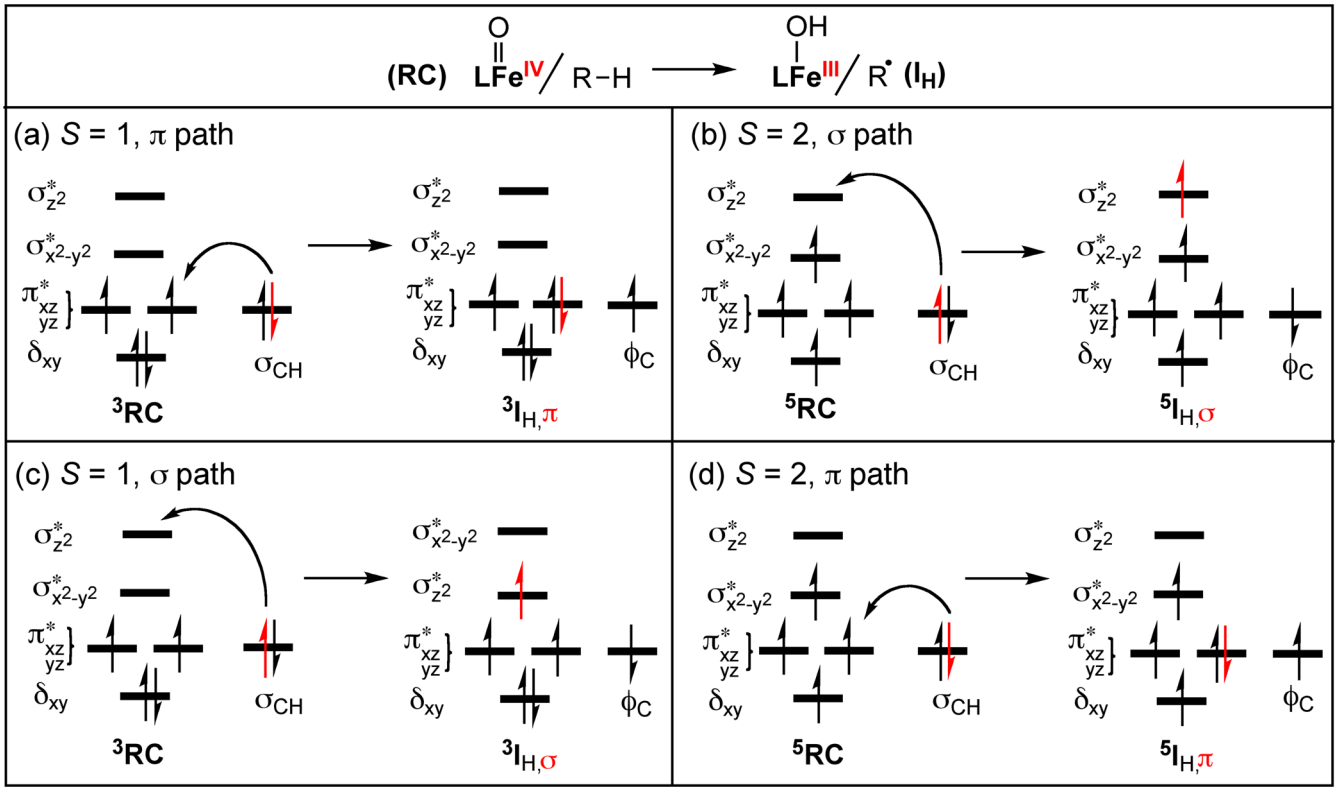

FIGURE 3. Electron-shift diagrams describing electronic reorganizations in the d- and σ_{CH}-orbitals, during HAT pathways for LFe^{IV}O/R-H, in S = 1 (a,c) and S = 2 (b,d).

two features is the EER in the HAT step versus the exchange saturation in the follow-up step.[15]

These findings of a favored spin state abound, for example, for oxoiron,[5,17] nitridoiron,[3d,18] oxochromium,[19] and oxomanganese[20,21] complexes reacting with alkanes and olefins. What makes certain spin states favored over others?

Exchange-Enhanced Reactivity

The above trends are associated with exchange interactions.[22,23] Consider two electrons in two d orbitals. Whenever these electrons have identical spins, the electron–electron repulsion is reduced compared with opposite-spin electrons. This reduction is expressed by the exchange interaction term, K_{dd}, which varies with the spatial extension of the d-orbitals and their delocalization onto the ligands.[9,22,23]

Figure 2 shows trends of K_{dd} values. Figure 2a shows that K_{dd} gets larger as the transition metal changes from left-to-right in a period, whereas stepping down a column decreases K_{dd}.[22] Figure 2b shows $K_{dd}(MO^+)/K_{dd}(M^+)$, the ratio of K_{dd} for an OMC to the bare-metal cation.[9,23] In the

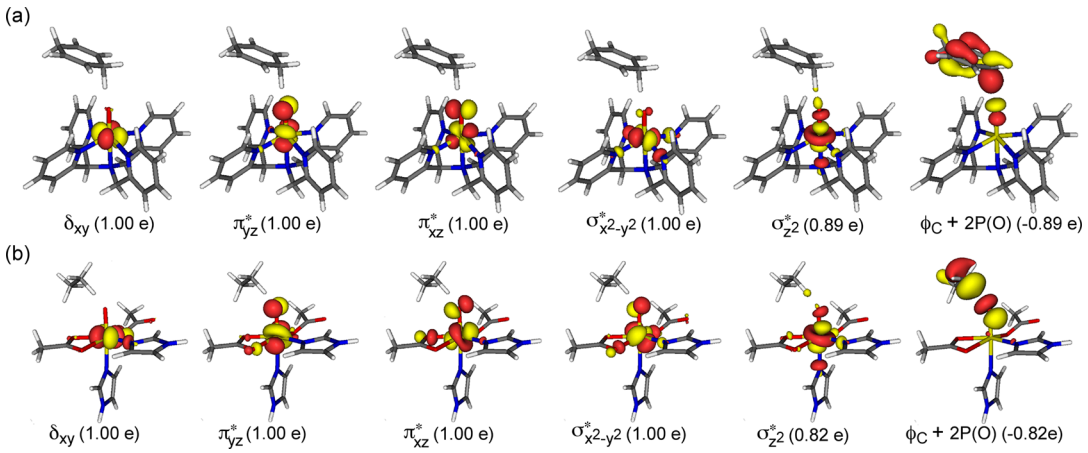

FIGURE 4. SNOs of $^5TS_{H,\sigma}$ species and their occupancies (in parentheses): (a) **2/S2** and (b) **16/S12**. The negative occupation number signifies a β-spin electron.

first half of the first-row transition metals, where the d-type orbitals are more localized on the metal, the ratio is closer to 1, while in the latter half it drops. In the 4d metals, $K_{dd}(MO^+)/K_{dd}(M^+)$ is ~0.5.[23] Clearly, exchange will matter more for 3d metals, and may increase as the metal-oxo bond gets elongated during the reaction. These trends carry over to nitridometal complexes.

Counting Exchange Interactions During Bond Activation. A useful mnemonic for tracking the number of K_{dd}'s is the electron-shift diagram,[6b−d,8b,9,13,16] exemplified in Figure 3 for HAT whereby the oxidant changes from $Fe^{IV}O$ to $Fe^{III}OH$, and the alkane R−H to a radical R·. Hence, the iron d-orbitals gain one electron during HAT. This can be viewed as a concerted proton-coupled electron transfer (PCET),[9,13] whereby the electron of H· shifts to a d orbital, while H^+ makes a bond to a lone pair on the oxo ligand.

Figure 3 shows generic HAT pathways: In Figure 3a (S = 1), a β-spin electron shifts to the $\pi^*_{xz/yz}$ d-orbital, leaving behind $^2Fe^{III}OH$, ferromagnetically coupled to an α-electron of the radical (in ϕ_C). Figure 3b shows the same process for S = 2, wherein an α-electron shifts to σ^*_{z2}, generating $^6Fe^{III}OH$ antiferromagnetically coupled to R·. Similarly, Figure 3c,d shows the alternative S = 1 and S = 2 paths, wherein the electron shifts to σ^*_{z2} and $\pi^*_{xz/yz}$, respectively.

Inspection of the $LFe^{III}OH$ moieties shows that, in Figure 3b, the PCET increases the number of exchange interactions by $4K_{dd}$ units, while in Figure 3d it depletes the exchange stabilization by $3K_{dd}$ units. Similarly, in Figure 3a, the exchange stabilization decreases by $1K_{dd}$, while in Figure 3c it increases by $2K_{dd}$. Therefore, in exchange-only terms, the most favored process is Figure 3b. However, this process involves also promotion energies within the d-block orbitals, relative to the S = 1 processes. Therefore, the balance of the exchange-energy change (ΔK_{dd}) versus the orbital promotion energy (ΔE_{orb}) will determine the energy ordering of the $^{3,5}I_H$ intermediates for the processes in Figure 3.

Computed K_{dd} values for FeO complexes are typically 9.3−13.6 kcal/mol,[9] that is, ~12 kcal/mol on average. The values of $\Delta E_{orb}(\pi^*_{xz/yz} \rightarrow \sigma^*_{z2}/\delta_{xy} \rightarrow \sigma^*_{x2-y2})$ are sensitive to the ligands; for N5-ligands, $\Delta E_{orb} \sim 50-60$ kcal/mol,[7c,9] while for weaker-field ligands, for example, **16**, $\Delta E_{orb} \sim 29-37$ kcal/mol (see the Supporting Information), that is, ~50 kcal/mol on average. For $Fe^{III}OH/R\cdot$ where the Fe−O bond is long, ΔE_{orb} decreases by 10−20 kcal/mol (see the Supporting Information). Nevertheless, for simplicity, we use the average values to predict the energy ordering for the $^{3,5}I_H$ intermediates in Figure 3.

$^5I_{H,\sigma}$ in Figure 3b is favored by $7K_{dd}$ units over $^5I_{H,\pi}$; in Figure 3d, this amounts to ~84 kcal/mol and exceeds ΔE_{orb}-$(\pi^*_{xz/yz} \rightarrow \sigma^*_{z2})$. Similarly, relative to $^3I_{H,\pi}$, $^5I_{H,\sigma}$ is stabilized by $10K_{dd}$ (~120 kcal/mol), which exceeds $\Delta E_{orb}(\pi^*_{xz/yz} \rightarrow \sigma^*_{z2} - \delta_{xy} \rightarrow \sigma^*_{x2-y2}) \sim 100$ kcal/mol. By contrast, vis-à-vis $^3I_{H,\pi}$, $^3I_{H,\sigma}$ is stabilized by $3K_{dd}$ (~36 kcal/mol), which is smaller than ΔE_{orb} (~50 kcal/mol). Thus, the $^{2S+1}I_H$ species in HAT processes of many oxoiron(IV) complexes will assume the following order: $E(^5I_{H,\sigma}) < E(^3I_{H,\pi}) < E(^5I_{H,\pi}) \sim E(^3I_{H,\sigma})$, in agreement with theoretical results.[13,16] As such, the $\Delta E_{orb}/\Delta K_{dd}$ balance *determines the thermodynamic driving force* of HAT during alkane hydroxylation, *and creates a favored state that has specific spin and unique electronic structure.*

These considerations apply also to the corresponding TSs. Figure 4 shows the spin-natural orbitals (SNOs)[13] of $^5TS_{H,\sigma}$ during HAT for **2/S2** and **16/S12**.[13,15] It is seen that the d-orbitals gain an electron[4c,6b] and they contain ~5 α-spin electrons (4.82−4.89), while a β-spin electron resides in a ϕ_{CHO} orbital, in accord with the electron-shift diagram in

Figure 3b. As such, the electron-shift diagram in Figure 3 is portable and can predict trends in TS as well.

Since the Fe−O bond in TS_H is longer than in the $Fe^{IV}O$ reactant, the $\Delta E_{orb}(TS_H)$ value decreases. As such, the TS_H species can be organized based on the balance of the exchange and orbital-promotion terms, which lead to the same order as obtained for $^{2S+1}I_H$, namely, that $^5TS_{H,\sigma}$ is the lowest energy species, followed by $^3TS_{H,\pi}$ and then by $^5TS_{H,\pi}$ and $^3TS_{H,\sigma}$.

Furthermore, $^5TS_{H,\sigma}$ (Figure 4a) is stabilized relative to the reactant cluster ^5RC by $4K_{dd}$ units (~48 kcal/mol), while $^3TS_{H,\pi}$ is depleted relative to ^3RC by $1K_{dd}$ (~12 kcal/mol). Thus, *the barrier on the EER state (S = 2) will be smaller than the barrier on the exchange-depleted state (S = 1).*

Figure 5 shows computational results for these TS_H species calculated for **2**/**S2**[13] and **1**/**S12**.[16] Clearly, the $\Delta E_{orb}/\Delta K_{dd}$ balance predicts the energy ordering and shows that the exchange-enhanced $^5TS_{H,\sigma}$ species has the lowest energy, and that the barrier on the EER state is significantly smaller than on the exchange-depleted state, S = 1. Sophisticated ab initio calculations reproduce the lower energy of $^5TS_{H,\sigma}$ versus $^3TS_{H,\pi}$.[16,24]

Furthermore, the specific results in Figure 5 are generally encountered in our group (Scheme 2)[5,6,13,15,24] and elsewhere,[7,8,16] thus unequivocally supporting the preference of the EER state. *This may be the reason for the abundance of nonheme enzymes which possess S = 2 oxoiron(IV) active species*. Experimental studies[17,25] convincingly demonstrated the superiority of S = 2 $Fe^{IV}O$ centers.

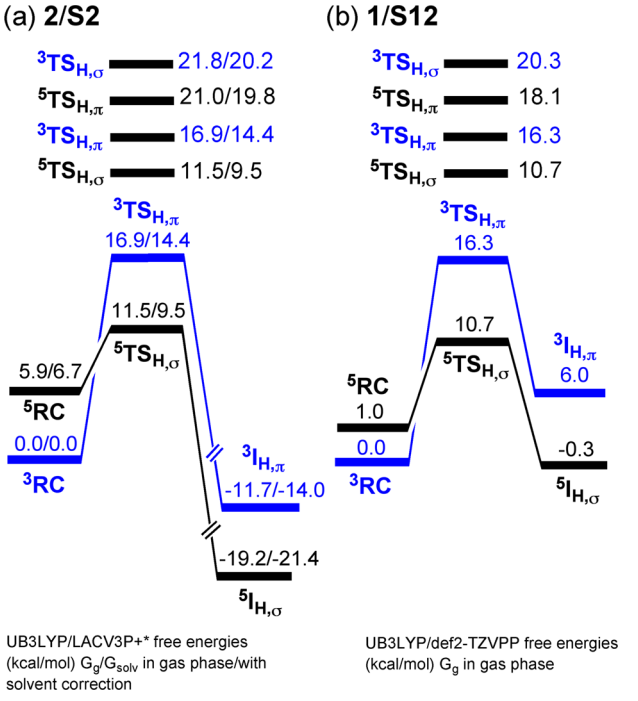

FIGURE 5. $^{2S+1}TS_{H,\sigma/\pi}$ energy ordering for (a) **2**/**S2**[13] and (b) **1**/**S12**.[16] The lowest energy profiles are depicted underneath.

Orbital-Selection Rules

The electron-shift diagrams lead to spin-dependent stereochemical predictions of the TS trajectories.[6b,13,15] Thus, a TS will adopt the geometry/trajectory that maximizes the overlap of the two orbitals that participate in the electron shift during the formation of the TS from the reactants.

Based on Figure 3, in S = 1 the electron shifts from σ_{CH} to $\pi^*_{xz/yz}$, and hence, $^3TS_{H,\pi}$ is predicted to prefer a sideways orientation that maximizes the $\sigma_{CH}-\pi^*_{xz/yz}$ overlap. However, during the formation of $^5TS_{H,\sigma}$, an electron shifts from σ_{CH} to σ^*_{z2}. Therefore, $^5TS_{H,\sigma}$ is predicted to assume an upright orientation that maximizes the $\sigma_{CH}-\sigma^*_{z2}$ overlap. The overlap cartoons are displayed in Figure 6a.

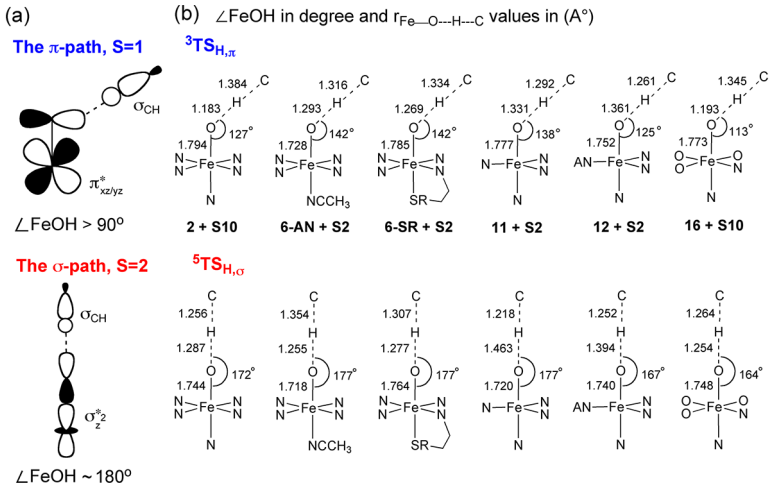

FIGURE 6. (a) Orbital-overlap cartoons predicting the orientations of $^3TS_{H,\pi}$ and $^5TS_{H,\sigma}$ based on Figure 3. (b) TS geometries[5] for HAT reactions of oxidant/substrate pairs.

Figure 6b shows that the computed geometries follow the prediction. Thus, while being soft, still the FeOH angle in $^{3}TS_{H,\pi}$ is 113−142°, whereas for $^{5}TS_{H,\sigma}$ it is 164−177°. These common features[6−8,16,24,25] illustrate that exchange enhancement endows the TS with specific stereochemistry, typical of the electronic reorganization required to form this TS.

EER and Deformation Features of TSs. Figure 6b also shows key bond lengths. Thus, generally, the $^{5}TS_{H,\sigma}$ species are "earlier" than $^{3}TS_{H,\pi}$, exhibiting less C−H/Fe-O bond breakage and less O−H bond making. Apparently, exchange enhancement stabilizes $^{5}TS_{H,\sigma}$ by enabling it to assume an earlier geometry compared with the exchange-depleted

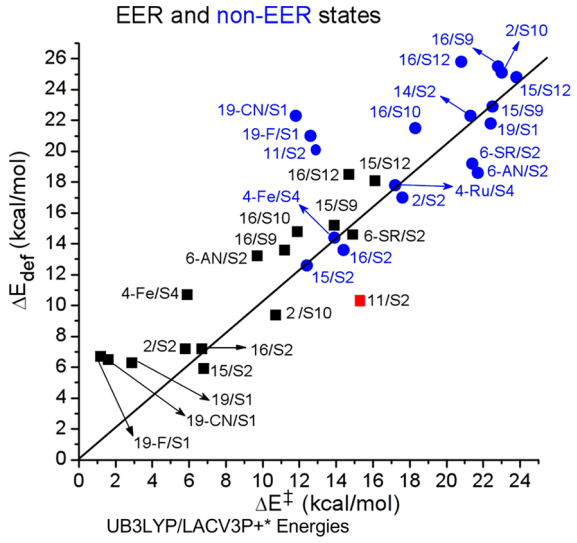

FIGURE 7. Plot of ΔE_{def} in $^{2S+1}TS_{H}$ species of various reactions versus the corresponding gas-phase barriers, $\Delta E^{\ddagger}$.

$^{3}TS_{H,\pi}$ species. *Hence, the generally observed*[6,13,15,21,26] *Hammond effect*[27] *for the geometry of* $^{5}TS_{H,\sigma}$ *originates in the exchange-enhanced stabilization of this TS.*

Figure 7 shows energetic manifestation of the Hammond effect by plotting the deformation energy of the reactants in the TS, ΔE_{def}, against the corresponding gas-phase barrier, $\Delta E^{\ddagger}$. The reactions include various oxidants and substrates, taken from Scheme 2.[5,6d,13,15,21] The line in Figure 7 has a slope of unity, such that a TS that has a higher deformation energy than the corresponding barrier lies above the line, while the opposite holds for TSs below the line. Black boxes represent the EER states (S = 2 for all $Fe^{IV}O$ cases and S = 1 for $Mn^{V}O$), while blue circles represent the exchange-depleted states. It is seen that most of the cases lie close to or above the line, namely, $\Delta E_{def} \geq \Delta E^{\ddagger}$. This in turn means that *the barrier generally derives from the deformation energies of the reactants in the TS* rather than from any interaction between them.

Figure 7 leads to two conclusions: First, since most reactions maintain $\Delta E_{def} \geq \Delta E^{\ddagger}$, there is then no need to invoke also steric effects to explain the barriers. This means that steric repulsions are manifested here as greater TS-deformation energies. The only case where steric effects appear explicitly is the reaction of $[(TMG_3tren)Fe^{IV}(O)]^{2+}$, **11**, with **S2** in S = 2 (red box, Figure 7),[6d] which despite the available exchange-enhanced interaction, still has a barrier higher than ΔE_{def}. The presence of steric hindrance[28] for **11** was demonstrated by Que et al.,[29] using **12**, which reacts faster than **11** due to the greater access to the substrate. Second, Figure 7 shows that *exchange-enhanced stabilization enables the corresponding reactions to establish TSs at a lower deformation energy*

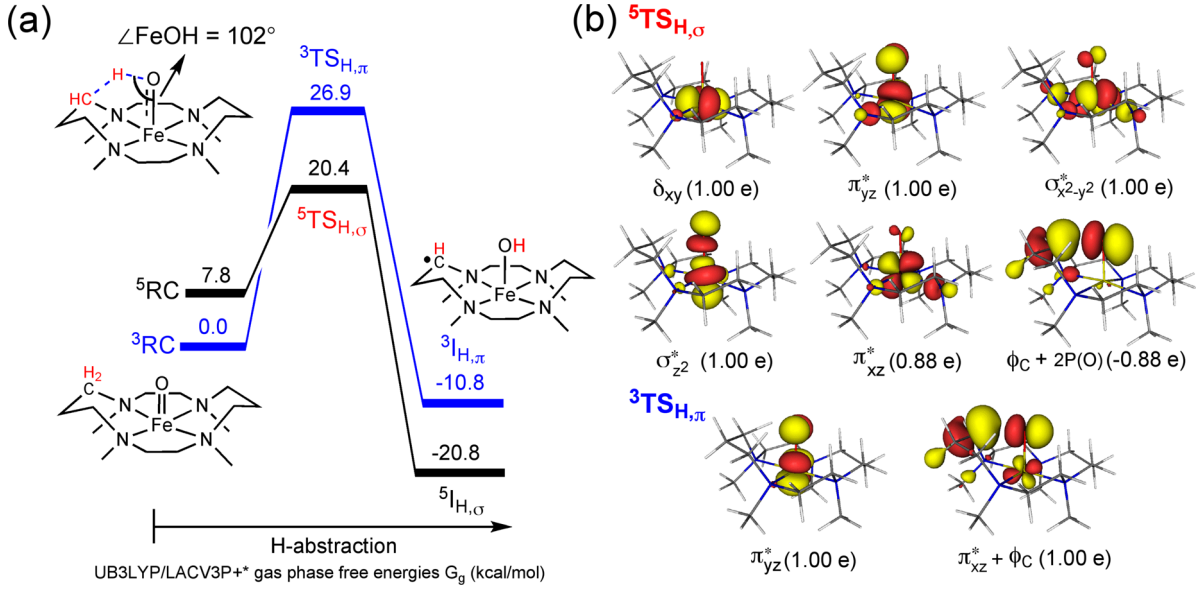

FIGURE 8. (a) S = 1,2 energy profiles for intramolecular HAT in **6-Fe**. (b) SNOs and their occupations (in parentheses) for $^{5}TS_{H}$ and $^{3}TS_{H}$.[30]

cost compared with the corresponding cases for the exchange-depleted TSs.

Is EER a Strong Rule?

Intramolecular decay of $Fe^{IV}O$ complexes like **6**–**9**[30] provides a test of the strength of the EER concept, because the structural constraints prevent the formation of $^5TS_{H,\sigma}$ with an upright orientation. Thus, if the $\sigma_{CH}-\sigma^*_{z2}$ orbital interaction (Figure 6) is the key factor of ^5TS_H stability, we may expect that $^5TS_{H,\sigma}$ will have to revert to the higher $^5TS_{H,\pi}$ species,[16] as indeed reported for some cases.[7b,8c] If however, the exchange is dominant, we may expect then to find $^5TS_{H,\sigma}-$ type species despite the constraint of $\angle$Fe–O–H to ~100°.

The energy profiles for intramolecular HAT in **6-Fe** in Figure 8a show that ^5TS_H lies below ^3TS_H by 6.5 kcal/mol. Figure 8b reveals that ^5TS_H contains ~5 α-spin electrons in the d-orbitals and one β-spin electron on the C–H–O moiety. This electronic structure follows the predictions of the electron-shift diagram (Figure 3b) for $^5TS_{H,\sigma}$. Similarly, ^3TS_H is the exchange-depleted $^3TS_{H,\pi}$ species. This is one of many cases, which behave similarly.[30] As such, $^5TS_{H,\sigma}$ that maximizes the exchange on iron materializes despite the severe structural constraints. This in turn means that *the exchange-enhanced stabilization overrides the overlap constraints*. EER is a strong rule; it stabilizes the corresponding TS even when the overlap with the σ^*_{z2} orbital is poor.

Scope of EER

While the EER state for $Fe^{IV}O$ complexes is high-spin S = 2, the high-spin S = 5/2 state of FeO^+ (**17**) has a high HAT barrier.[11] By contrast, the S = 5/2 state of $Por^{\bullet+}Fe^{IV}O$ (**18**), which consists of S = 2 $Fe^{IV}O$ coupled ferromagnetically to S = 1/2 $Por^{\bullet+}$, exhibits tiny HAT barriers.[6c] $Ru^{IV}O$ complexes, **4**-Ru, **6**-Ru, and **13**-Ru, show generally S = 1

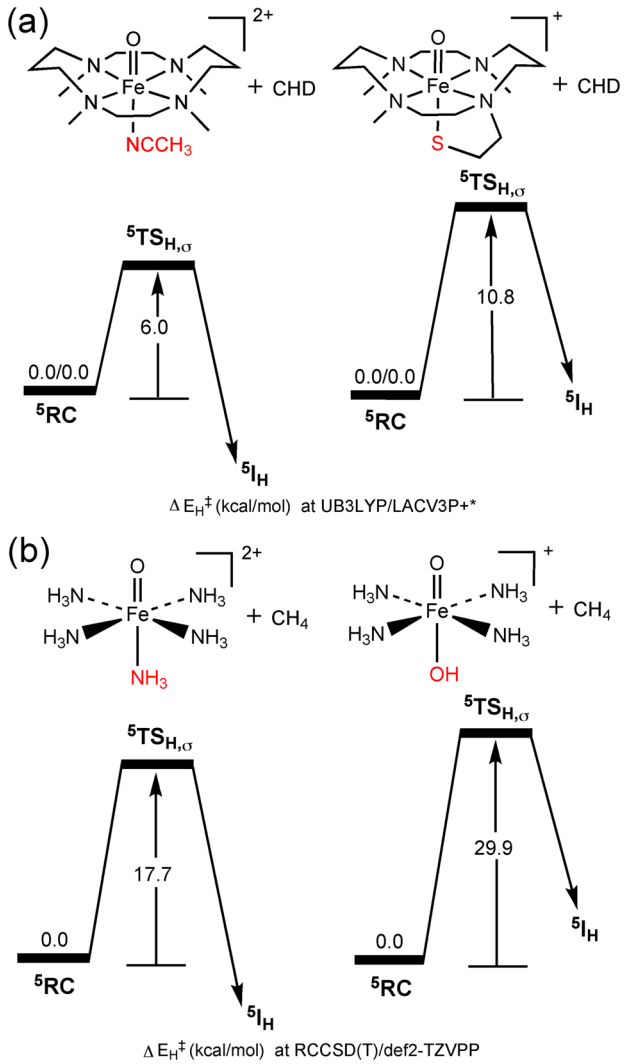

FIGURE 9. Axial-ligand effects on barriers of the EER states for (a) **6-AN**/**S2** and **6-SR**/**S2**[5,26] and (b) **1**/**S14** and **5**/**S14**.[24]

SCHEME 3. d-Orbital Occupancies in Several S = 5/2 Complexes

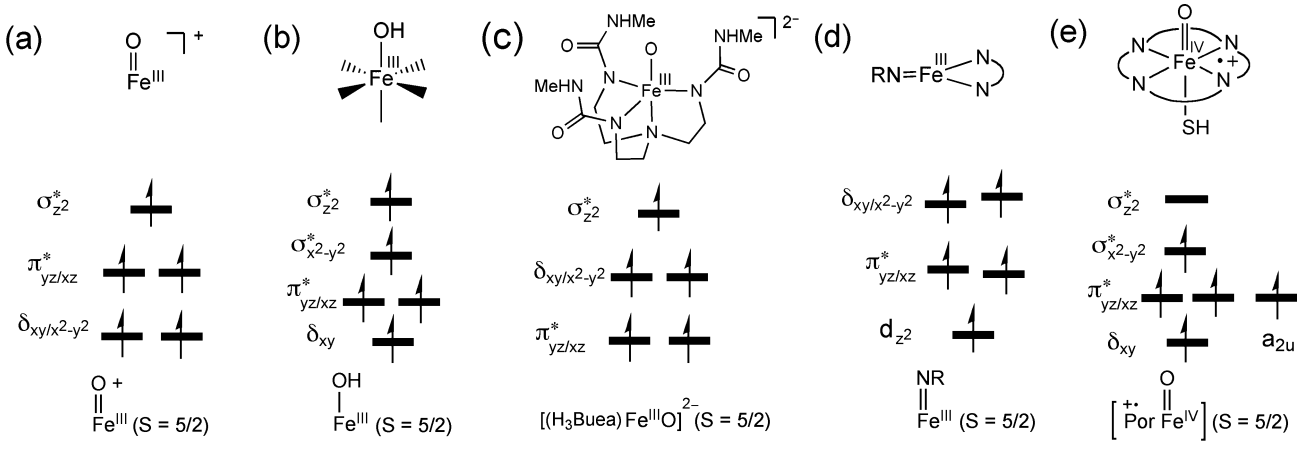

reactivity with high barriers;[3c,31,32] the corresponding S = 2 is much too high to matter.[5,31] Let us therefore elaborate on the scope of EER.

Axial Ligand Effects. Baerends et al.[7a] predicted the HAT-barrier dependence on the σ^*_{z2}-orbital energy, upon axial-ligand variation. The electron-shift diagram (Figure 3b) provides a similar rationale for the dependence of barriers on the axial ligand of nonheme $Fe^{IV}O$ reagents. Thus, as $^5TS_{H,\sigma}$ is generated by shifting an electron to σ^*_{z2}, the height of the S = 2 barrier is expected to increase as the axial ligand becomes a more powerful electron-donor that raises σ^*_{z2}. Figure 9 shows that changing the axial ligand in **6** from CH_3CN to $CH_2CH_2S^-$ raises the S = 2 HAT barrier,[5,26] and a change from NH_3 in **1** to the more basic HO^- ligand in **5** raises the barrier by 12.2 kcal/mol.[24] Thus, powerful electron donors as axial ligands diminish the EER advantage.

Exchange Saturation. Not every high-spin state enjoys EER. Scheme 3 shows electronic structures for reagents with S = 5/2 states. Scheme 3a shows the ground S = 5/2 state of the diatomic FeO^+; Scheme 3b shows the S = 5/2 moiety of $L_5Fe^{III}OH$, which is part of the $^5I_{H,\sigma}$ intermediate (Figure 1) or can model the reactive species of lipoxygenase;[33] Scheme 3c shows the $[(H_3Buea)Fe^{III}O]^{2-}$ complex,[34] **14**; and Scheme 3d shows an $Fe^{III}NR$ type reagent.[35] These are contrasted in Scheme 3e with the S = 5/2 excited state of the P450 reagent $(Por^{\bullet+})(SH)Fe^{IV}O$.[6c] It is seen that, in Scheme 3a–d, the S = 5/2 species contains Fe^{III} with a half-filled d-orbital block, which is *exchange-saturated*. Addition of an electron during an oxidation step will cause *a loss* of $4K_{dd}$ in the corresponding TS, and therefore, these species are not expected to be highly reactive. Indeed, FeO^+(S = 5/2) is unreactive.[11] $L_5Fe^{III}OH$ is not as reactive as $L_5Mn^{III}OH$ (d^4, S = 2).[33] Exchange saturation is also the reason why the thermodynamically favorable second HAT by $Fe^{III}OH$ leading to desaturation (Figure 1) has almost the same barrier as the first HAT which is nascent from the EER S = 2 state.[5,15] Similarly, $[(H_3Buea)Fe^{III}O]^{2-}$ activates only substrates with weak C–H bonds,[34] and the S = 5/2 state of $Fe^{III}NR$ complexes[35] is also a sluggish H-abstractor. By contrast, the S = 5/2 state of $(Por^{\bullet+})(SH)Fe^{IV}O$ is intrinsically reactive[6c] because the d-orbital block of its $Fe^{IV}O$ center is not exchange-saturated and will exhibit EER.

Figure 10 shows that the HAT barrier for the reaction of the exchange-saturated $[(H_3Buea)Fe^{III}O]^{2-}$ complex with CHD[34] is considerably higher than those for the EER states in Figures 1 and 5, wherein $Fe^{IV}O$ complexes activate much stronger C–H bonds.

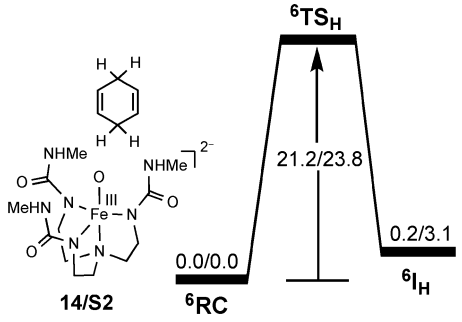

UB3LYP/LACV3P+* free energies (kcal/mol) G_g/G_{solv} in gas phase/ with solvent correction

FIGURE 10. DFT computed HAT barrier (kcal/mol) for **14-Fe/S2**.[5]

Generalization to other OMCs

As seen above, manifestations of EER depend on the d-electron count on the metal.

High d-Electron Count. Fe^{IV} with d^4 has maximal EER advantage in S = 2 with four unpaired electrons. Complexes with d^n configurations where $n > 4$ will experience low reactivity due to exchange depletion.[22,36] Therefore, EER in Co and Ni[37,38] will be observed if complexes can be prepared[3e] with oxidation states of V and VI, respectively.

Low d-Electron Count. High-valent early transition-metal complexes have too few d-electrons to confer EER.[9] For example, LCr^VO complexes have d^1 configurations, and hence EER, will not be manifested during the bond-activation step. The exchange stabilization will commence during rebound, when $LCr^{IV}OH$ is converted to $LCr^{III}(ROH)$ and the d-orbital block is enriched by two d-electrons.[9,19] The minimum number of d-electrons for which the bond-activation step still exhibits EER is d^2 as typically found in Mn^VO complexes.

Figure 11 summarizes the HAT reactivity of **19-X**, $[Cz(X)Mn^VO]$, with DHA, **S1**.[21] Figure 11a shows that the S = 1 ($\delta^1\pi^*_{xz/yz}{}^1$) state enjoys EER, starting above S = 0 but becoming the ground state for TS_H and I_H due to gain of $3K_{dd}$ relative to the S = 0 species. It is the S = 1 state that leads to the observed[39] dramatic axial-ligand effect on reactivity. Figure 11b shows that DFT calculations[21] reproduce the experimental barrier-lowering effect of the electron-rich ligands. Groves's[20b] pioneering study provided evidence for the importance of this excited state. Eisenstein et al.[20a] emphasized its oxyl-radical character.

Second and Third Row Complexes. $Ru^{IV}O$ is an example where the K_{dd} shrinkage (Figure 2) and increased orbital-energy gaps disable EER.[31,32] Figure 12 shows that the S = 2 state for $Ru^{IV}O$ is high-lying throughout the bond activation

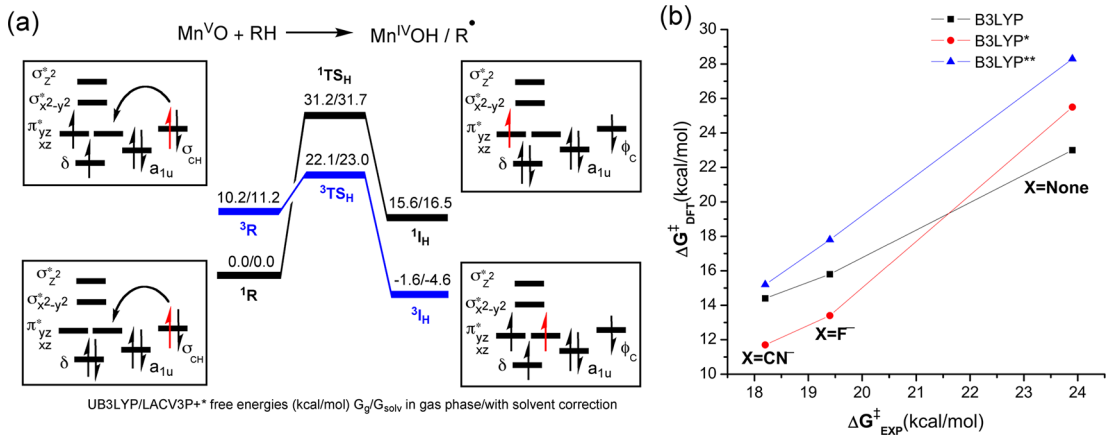

FIGURE 11. (a) DFT[21] energy profile for HAT in **19** (X = none)/**S1**, with electron-shift diagrams for S = 0 and S = 1. (b) Computed $\Delta G^{\ddagger}$ values versus experimental ones for **19-X** (X = none, F^-, CN^-)/**S1**.

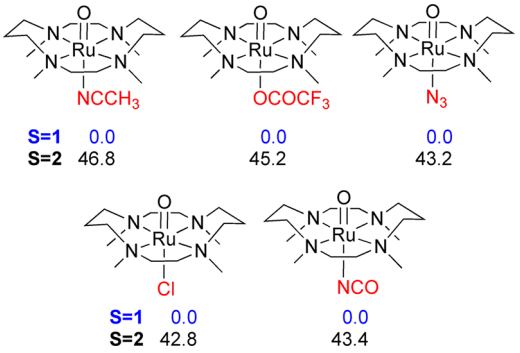

FIGURE 12. S = 1/S = 2 relative energies (kcal/mol) for **6-Ru**(X).[31]

SCHEME 4. Electron-Shift Diagrams for OAT[26]

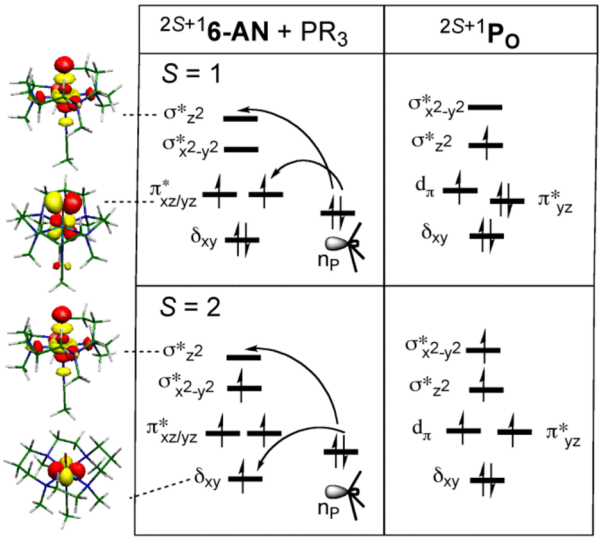

phase. Note that S = 2 may exhibit EER in photochemistry of $Ru^{IV}O$ complexes.

Concerted 2e-Processes. The above discussions apply also to olefin epoxidation, which, like alkane activation, involves two consecutive one-electron steps. By contrast, OAT (Scheme 4) is a concerted two-electron process[26] that conserves the number of exchange interactions and does not enjoy EER. Indeed, it is observed[17a,25,31] that HAT by oxoiron(IV) complexes benefits from the advent of the S = 2 state, whereas OAT to phosphines shows little benefit, if any. In fact, OAT responds to the electrophilicity of the oxoiron-(IV) reagent.[26,31] The same holds true for $Mn^{V}O$ complexes.[40] The reason that $Fe^{IV}O$ reagents abstract hydrogen *rather than inserting into C–H bonds is that the latter 2e-process does not enjoy EER.*

SCHEME 5. Spin Crossover Scenarios:[6b,26] (a) Spin Pre-Equilibrium (b) Crossover En Route to the ^5TS_H with Spin-Inversion Probability (SIP) < 1 Marked As Dashed Arrow

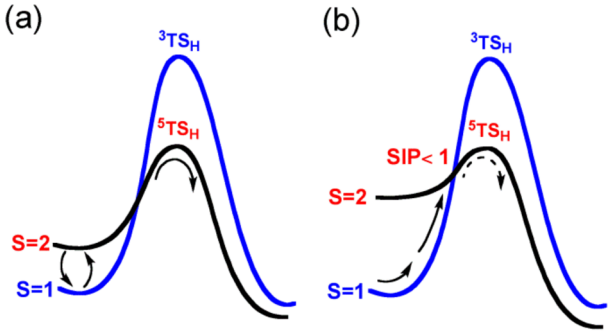

Mechanistic Considerations. Spin crossover[11,41,42a] affects reactivity. Scheme 5 shows a generic HAT reaction with two states.[6b,26] Scheme 5a describes a case where the small initial spin-state gap results in fast spin pre-equilibrium.[6b,26,42b] Consequently, the reaction proceeds via ^5TS_H, and the spin crossover confers EER catalysis of HAT. Scheme 5b describes large spin-state gaps where the spin crossover will occur en route to ^5TS_H. As was shown in an extensive study,[41a] such a late spin-crossover event is typified by a depleted

spin−orbit coupling and poor spin-inversion probability[41a] (SIP). This will downsize the EER effect.[6b,26]

Our[5,6b,21,26] minimum-energy crossing-point (MECP)[42a] calculations reveal the two scenarios (see the Supporting Information). For example, in the reaction **19/S1**, the MECP coincides with the TS geometry of the EER state.[21] However, for the reactions described in Figure 9a, **6-AN** exhibits a high-energy MECP en route to ^5TS_H, while **6-SR** with the small spin-state gap may follow a pre-equilibrium scenario. The findings that the calculated[5,26] HAT barrier for **6-SR** is larger than that for **6-AN**, whereas experiment shows that **6-SR** is more reactive,[43] led us to conclude[26] that the HAT reactions of **6-SR** proceed with SIP = 1, while those of **6-AN** with SIP < 1 due to depleted spin−orbit coupling.[41a] Clearly, rigorous treatments of the spin crossover issues will be necessary to reveal when does EER fully manifest and when is it downsized by poor SIP.

Prospects

The EER concept and orbital-selection rules provide a framework for understanding of bioinorganic oxidation reactions. Thus, we show that exchange controls the thermodynamic driving force, the reaction barrier, and the TS structure. It also rationalizes *the prevalence of stepwise mechanisms over concerted insertions into C−H/C=C bonds,* and the ubiquity of high-spin oxoiron(IV) complexes in enzymes.[1,3a−3e] Since the relative exchange stabilization is responsible for the relative stability of the various intermediates during the HAT step (e.g., Figure 5), EER will generally coincide with the Bell−Evans−Polanyi (BEP) principle, which was demonstrated by Mayer[44] and others[6b,8b,21,34] to rationalize HAT reactivity. However, by itself, this principle cannot account[26] for the variety of reactivity patterns discussed here, for example, the TS structure or the preference of HAT despite the thermodynamic preference of C−H insertion, and so forth.

The concepts described above are portable and allow making predictions on less studied areas. For example, the use of oxo-lanthanide and oxo-actinide complexes may reveal if f-orbitals can constitute a sink for the added electron during oxidation and thereby leading to EER. Similarly, high-valent $Co^{V}O$ and $Ni^{VI}O$ complexes are promising EER candidates. Finally, 4d and 5d OMCs may reveal EER in the excited state, thus extending the horizons of the concept.

Supporting Information. Additional references, tables of K_{dd}, ΔE_{orb}, and ΔE_{def} values, a figure of MECP calculations, and Cartesian coordinates. This material is available free of charge via the Internet at http://pubs.acs.org.

Support by the ISF (53/09) is acknowledged.

BIOGRAPHICAL INFORMATION

Dandamudi Usharani is a postdoctoral associate in Jerusalem, and a graduate of University of Hyderabad (2009). Her major interests are in metallo-enzymes.

Deepa Janardanan is a postdoctoral associate in Jerusalem, and a graduate of IIT Mumbai (2009). Her major interest is in transition-metal chemistry.

Chunsen Li is a postdoctoral associate in Jerusalem, and a graduate of Xiamen University (2007). His major interests are in metallo-enzymes.

Sason Shaik is the Director of the Lise Meitner-Minerva Center in Jerusalem. Among his interests are concepts for bonding and reactivity.

FOOTNOTES

*To whom correspondence should be addressed. Telephone: +972 (0)2 658 5909. Fax +972 (0)2 658 4033. E-mail: sason@yfaat.ch.huji.ac.il.
The authors declare no competing financial interest.

REFERENCES

1 (a) van Eldik, R. Inorganic and Bioinorganic Mechanisms. *Chem. Rev.* **2005**, *105*, 1917–1921. (b) Krebs, C.; Fujimori, D. G.; Walsh, C. T.; Bollinger, J. M., Jr. Non-Heme Fe(IV)-Oxo Intermediates. *Acc. Chem. Res.* **2007**, *40*, 484–492. (c) Jin, Y.; Lipscomb, J. D. Desaturation Reactions Catalyzed by Soluble Methane Monooxygenase. *J. Biol. Inorg. Chem.* **2001**, *6*, 717–725. (d) Nam, W. Dioxygen Activation by Metalloenzymes and Models. *Acc. Chem. Res.* **2007**, *40*, 465–634.

2 Bollinger, J. M., Jr.; Krebs, C. Enzymatic C-H Activation by Metal-Superoxo Intermediates. *Curr. Opin. Chem. Biol.* **2007**, *11*, 151–158.

3 (a) Que, L., Jr. The Road to Nonheme Oxyferryls and Beyond. *Acc. Chem. Res.* **2007**, *40*, 493–500. (b) Nam, W. High-Valent Iron(IV)-Oxo Complexes of Heme and Nonheme Ligands in Oxygenation Reactions. *Acc. Chem. Res.* **2007**, *40*, 522–531. (c) Benet-Buchholz, J.; Comba, P.; Llobet, A.; Roeser, S.; Vadivelu, P.; Wadepohl, W.; Wiesner., S. Iron vs. Ruthenium − A Comparison of the Stereoselectivity in Catalytic Olefin Epoxidation. *Dalton Trans.* **2009**, 5910–5923. (d) Hohenberger, J.; Ray, K.; Meyer, K. The Biology and Chemistry of High-valent Iron-Oxo and Iron-Nitrido Complexes. *Nature Commun.* DOI: 10.1038/ncomms1718. (e) Winkler, J. R.; Gray, H. B. Electronic Structure of Oxo-Metal Ions. *Struct. Bonding (Berlin, Ger.)* **2012**, *142*, 17–28.

4 (a) Siegbahn, P. E. M.; Borowski, T. Modeling Enzymatic Reactions Involving Transition Metals. *Acc. Chem. Res.* **2006**, *39*, 729–738. (b) Michel, C.; Baerends, E. J. What Singles out the FeO^{2+} Moiety? A Density-Functional Theory Study of the Methane-to-Methanol Reaction Catalyzed by the First Row Transition-Metal Oxide Dications $MO(H_2O)p^{2+}$, M = V-Cu. *Inorg. Chem.* **2009**, *48*, 3628–3638. (c) Ye, S.; Neese, F. Quantum Chemical Studies of C-H Activation reactions by High-Valent Nonheme Iron Centers. *Curr. Opin. Chem. Biol.* **2009**, *13*, 89–98. (d) Solomon, E. I.; Wong, S. D.; Liu, L. V.; Decker, A.; Chow, M. S. Peroxo and Oxo Intermediates in Mononuclear Nonheme Iron Enzymes and Related Active Sites. *Curr. Opin. Chem. Biol.* **2009**, *13*, 99–113.

5 A full list of the references for Scheme 2 is in the Supporting Information.

6 For descriptions of exchange-enhanced reactivity, see: (a) Kumar, D.; Hirao, H.; Que, L., Jr.; Shaik, S. Theoretical Investigation of C-H Hydroxylation by $(N4Py)Fe^{IV}=O^{2+}$: An Oxidant More Powerful than P450? *J. Am. Chem. Soc.* **2005**, *127*, 8026–8027. (b) Hirao, H.; Kumar, D.; Que, L., Jr.; Shaik, S. Two-State Reactivity in Alkane Hydroxylation by Non-Heme Iron Oxo Complexes. *J. Am. Chem. Soc.* **2006**, *128*, 8590–8606. (c) Hirao, H.; Kumar, D.; Thiel, W.; Shaik, S. Two-States and Two More in the Mechanisms of Hydroxylation and Epoxidation by Cytochrome P450. *J. Am. Chem. Soc.* **2005**, *127*, 13007–13018. (d) Janardanan, D.; Wang, Y.; Schyman, P.; Que, L., Jr.; Shaik, S. The Fundamental Role of Exchange-Enhanced Reactivity in C−H Activation by S=2 Oxo Iron(IV) Complexes. *Angew. Chem., Int. Ed.* **2010**, *49*, 3342–3345.

7 For frontier-orbital modeling of the exchange-stabilizing effect, see: (a) Bernasconi, L.; Louwerse, M. J.; Baerends, E. J. The Role of Equatorial and Axial Ligands in Promoting the Activity of Non-Heme Oxidoiron(IV) Catalysts in Alkane Hydroxylation. *Eur. J. Inorg. Chem.* **2007**, 3023–3033. (b) Neidig, M. L.; Decker, A.; Choroba, O. W.; Huang, F.; Kavana, M.; Moran, G. R.; Spencer, J. B.; Solomon, E. I. Spectroscopic and Electronic Structure Studies of Aromatic Electrophilic Attack and Hydrogen-atom Abstraction by Non-heme Iron

Enzymes. *Proc. Natl. Acad. Sci. USA.* **2006**, *103*, 12966–12973. (c) Decker, A.; Rohde, J.-U.; Klinker, E. J.; Wong, S. D.; Que, L., Jr.; Solomon, E. I. Spectroscopic and Quantum Chemical Studies on Low-Spin Fe^{IV}═O Complexes: Fe−O Bonding and Its Contributions to Reactivity. *J. Am. Chem. Soc.* **2007**, *129*, 15983–15996.

8 (a) Johansson, A. J.; Blomberg, M. R. A.; Siegbahn, P. E. M. Quantum Chemical Modeling of the Oxidation of Dihydroanthracene by the Biomimetic Nonheme Iron Catalyst $[(TMC)Fe^{IV}(O)]^{2+}$. *J. Phys. Chem. C* **2007**, *111*, 12397–12406. (b) de Visser, S. P. Propene Activation by the Oxo-iron Active Species of Taurine/α-ketoglutarate Dioxygenase (TauD) Enzyme. How Does the Catalysis Compare to Heme-enzyme? *J. Am. Chem. Soc.* **2006**, *128*, 9813–9824. (c) Hirao, H.; Morokuma, K. Ferric Superoxide and Ferric Hydroxide Are Used in the Catalytic Mechanism of Hydroxyethylphosphonate Dioxygenase: A Density Functional Theory Investigation. *J. Am. Chem. Soc.* **2010**, *132*, 17901–17909.

9 Shaik, S.; Chen, H.; Janardanan, D. Exchange-Enhanced Reactivity in Bond Activation by Metal-Oxo Enzymes and Synthetic Reagents. *Nat. Chem.* **2011**, *3*, 19–27.

10 (a) van Zeist, W.-J.; Bickelhaupt, F. M. The Activation Strain Model of Chemical Reactivity. *Org. Biomol. Chem.* **2010**, *8*, 3118–3127. (b) Kitaura, K.; Morokuma, K. A New Energy Decomposition Scheme for Molecular Interactions within the Hartree-Fock Approximation. *Int. J. Quantum Chem.* **1976**, *10*, 325–340.

11 Schröder, D.; Shaik, S.; Schwarz, H. Two-State Reactivity as a New Concept in Organometallic Chemistry. *Acc. Chem. Res.* **2000**, *33*, 139–145.

12 Kaizer, J.; Klinker, E. J.; Oh, N. Y.; Rohde, J.-U.; Song, W. J.; Stubna, A.; Kim, J.; Münck, E.; Nam, W.; Que, L., Jr. Nonheme $Fe^{IV}O$ Complexes That Can Oxidize the C-H Bonds of Cyclohexane at Room Temperature. *J. Am. Chem. Soc.* **2004**, *126*, 472–473.

13 Janardanan, D.; Usharani, D.; Chen, H.; Shaik, S. Modeling C-H Abstraction Reactivity of Fe(IV)O Oxidants with Alkanes: What Role do Counter Ions Play? *J. Phys. Chem. Lett.* **2011**, *2*, 2610–2617.

14 Comba, P.; Maurer, M.; Vadivelu, P. Oxidation of Cyclohexane by High-valent Iron Bispidine Complexes: Tetradentate versus Pentadentate Ligands. *Inorg. Chem.* **2009**, *48*, 10389–10396.

15 Usharani, D.; Janardanan, D.; Shaik, S. Does the TauD Enzyme Always Hydroxylate Alkanes, While an Analogous Synthetic Nonheme Reagent Always Desaturates them? *J. Am. Chem. Soc.* **2011**, *133*, 176–179.

16 Geng, C.; Ye, S.; Neese, F. Analysis of Reaction Channels for Alkane Hydroxylation by Nonheme Iron(IV)−Oxo Complexes. *Angew. Chem., Int. Ed.* **2010**, *49*, 5717–5720.

17 (a) Xue, G.; DeHont, R.; Münck, E.; Que, L., Jr. Million-fold Activation of the $[Fe_2(\mu\text{-}O)_2]$ Diamond Core for C-H Bond Cleavage. *Nat. Chem.* **2010**, *2*, 400–405. (b) Xue, G.; Pokutsa, A.; Que, L., Jr. Substrate-Triggered Activation of a Synthetic $[Fe_2(\mu\text{-}O)_2]$ Diamond Core for C-H Bond Cleavage. *J. Am. Chem. Soc.* **2011**, *133*, 16657–16667. (c) Donald, W. A.; McKenzie, C. J.; O'Hair, R. A. J. C-H Bond Activation of Methanol and Ethanol by a High-spin Fe(IV)O Biomimetic Complex. *Angew. Chem., Int. Ed.* **2011**, *50*, 8379–8383.

18 Klinker, E. J.; Jackson, T. A.; Jensen, M. P.; Stubna, A.; Juhász, G.; Bominaar, E. L.; Münck, E.; Que, L., Jr. A Tosylimido Analog of a Nonheme Oxoiron(IV) Complex. *Angew. Chem., Int. Ed.* **2006**, *45*, 7394–7397.

19 Brandt, P.; Norrby, P.-O.; Daly, A. M.; Gilheany, D. G. Chromium-Salen-Mediated Alkene Epoxidation: A Theoretical and Experimental Study Indicates the Importance of Spin-Surface Crossing and the Presence of a Discrete Intermediate. *Chem.—Eur. J.* **2002**, *8*, 4299–4307.

20 (a) Balcells, D.; Raynaud, C.; Crabtree, R. H.; Eisenstein, O. The Rebound Mechanism in Catalytic C-H Oxidation by MnO(tpp)Cl from DFT studies: Electronic Nature of the Active Species. *Chem. Commun.* **2008**, 744–746. (b) Jin, N.; Groves, J. T. Unusual Kinetic Stability of a Ground-State Singlet Oxomanganese(V) Porphyrin. Evidence for a Spin State Crossing Effect. *J. Am. Chem. Soc.* **1999**, *121*, 2923–2924.

21 Janardanan, D.; Usharani, D.; Shaik, S. The Origins of Dramatic Axial Ligand Effects: Closed-Shell Mn^{V}-Oxo Complexes Use Exchange-Enhanced Open-Shell States to Mediate Efficient H-Abstraction Reactions. *Angew. Chem., Int. Ed.* **2012**, *51*, 4421–4425.

22 Carter, E. A.; Goddard, W. A., III. Relationships Between Bond Energies In Coordinatively Unsaturated and Coordinatively Saturated Transition-Metal Complexes: A Quantitative Guide For Single, Double, And Triple Bonds. *J. Phys. Chem.* **1988**, *92*, 5679–5683.

23 Carter, E. A.; Goddard, W. A. III. Early- versus Late-Transition-Metal-Oxo Bonds: The Electronic Structure of VO^{+} and RuO^{+}. *J. Phys. Chem.* **1988**, *92*, 2109–2115.

24 Chen, H.; Lai, W. Z.; Shaik, S. Exchange-enhanced H-Abstraction Reactivity of High-Valent Non-Heme Iron(IV)-Oxo from Coupled Cluster and Density Functional Theories. *J. Phys. Chem. Lett.* **2010**, *1*, 1533–1540.

25 Seo, S. M.; Kim, N. H.; Cho, K.-B.; So, J. E.; Park, S. K.; Clémancey, M.; Garcia-Serres, R.; Latour, J.-M.; Shaik, S.; Nam, W. A Mononuclear Nonheme Iron(IV)-Oxo Complex which is More Reactive than Cytochrome P450 model Compound I. *Chem. Sci.* **2011**, *2*, 1039–1045.

26 Hirao, H.; Que, L., Jr.; Nam, W.; Shaik, S. A TSR Rationale for the Counterintuitive Axial Ligand Effect on the C-H Activation Reactivity of Nonheme Fe(IV)═O Oxidants. *Chem.—Eur. J.* **2008**, *14*, 1740–1756.

27 Hammond, G. S. A Correlation of Reaction Rates. *J. Am. Chem. Soc.* **1955**, *77*, 334–338.

28 England, J.; Martinho, M.; Farquhar, E. R.; Frisch, J. R.; Bominaar, E. L.; Münck, E.; Que, L., Jr. A Synthetic High-Spin Oxoiron(IV) Complex: Generation, Spectroscopic Characterization, and Reactivity. *Angew. Chem., Int. Ed.* **2009**, *48*, 3622–3626.

29 England, J.; Guo, Y.; Van Heuvelen, K. M.; Cranswick, M. A.; Rohde, G. T.; Bominaar, E. L.; Münck, E.; Que, L., Jr. A More Reactive Trigonal-Bipyramidal High-Spin Oxoiron(IV) Complex with a Cis-Labile Site. *J. Am. Chem. Soc.* **2011**, *133*, 11880–11883.

30 Mas-Ballesté, R.; McDonald, A. R.; Reed, D.; Usharani, D.; Schyman, P.; Milko, P.; Shaik, S.; Que, L., Jr. Intramolecular Gas Phase Reactions of Synthetic Non-heme Oxoiron(IV) Ions: Proximity and Spin-State Reactivity Rules. *Chem.—Eur. J.* **2012**, *18*, 11747–11760.

31 Dhuri, S. N.; Seo, M. S.; Lee, Y. M.; Hirao, H.; Wang, Y.; Nam, W.; Shaik, S. Experiment and Theory Reveal the Fundamental Difference between Reactivity Patterns in Nonheme Fe(IV)═O and Ru(IV)═O Oxidants. *Angew. Chem., Int. Ed.* **2008**, *47*, 3356–3359.

32 (a) For a recent debate on the reactive spin-sate of Ru(IV)O complexes, see: Schroder, D.; Shaik, S. Comment on "A Low-Spin Ruthenium(IV)-Oxo Complex: Does the Spin State Have an Impact on the Reactivity. *Angew. Chem., Int. Ed.* **2011**, *50*, 3850–3851. (c) Kojima, T.; Fukuzumi, S. Reply. *Angew. Chem., Int. Ed.* **2011**, *50*, 3852–3853. (b) Kojima, T.; Nakayama, K.; Ikemura, K.; Ogura, T.; Fukuzumi, S. Formation of a Ruthenium(IV)-Oxo by Electron-Transfer Oxidation of a Coordinatively Saturated Ruthenium(II) Complex and Detection of Oxygen Rebound Intermediates in C-H Bond Oxygenation. *J. Am. Chem. Soc.* **2011**, *133*, 11692–11700.

33 Goldsmith, C. R.; Stack, T. D. P. Hydrogen Atom Abstraction by a Mononuclear Ferric Hydroxide Complex: Insights into the Reactivity of Lipoxygenase. *Inorg. Chem.* **2006**, *45*, 6048–6055.

34 Gupta, R.; Borovik, A. S. Monomeric $Mn^{II/II}$ and $Fe^{III/II}$ Complexes with Terminal Hydroxo and Oxo Ligands: Probing Reactivity via O-H Bond Dissociation Energies. *J. Am. Chem. Soc.* **2003**, *125*, 13234–13242.

35 Cowley, R. E.; Eckert, N. A.; Vaddadi, S.; Figg, T. M.; Cundari, T. R.; Holland, P. L. Selectivity and Mechanism of Hydrogen Atom Transfer by an Isolable Imidoiron(III) Complex. *J. Am. Chem. Soc.* **2011**, *133*, 9796–9811.

36 Carroll, J. J.; Haug, K. L.; Weisshaar, J. C.; Blomberg, M. R. A.; Siegbahn, P. E. M.; Svensson, M. Gas Phase Reactions of Second-row Transition-Metal Atoms with Small Hydrocarbons: Experiment and Theory. *J. Phys. Chem.* **1995**, *99*, 13955–13969.

37 For a recent $Ni^{III}O(H)$ species: Pfaff, F. F.; Heims, F.; Kundu, S.; Mebs, S.; Ray, K. Spectroscopic Capture and Reactivity of S=1/2 Nickel(III)-Oxygen Intermediates in the Reaction of a Ni^{II}-salt with mCPBA. *Chem. Commun.* **2012**, *48*, 3730–3732.

38 For a putative $Co^{IV}O$: Pfaff, F. F.; Kundu, S.; Risch, M.; Pandian, S.; Heims, F.; Pryjomska-Ray, I.; Haack, P.; Metzinger, R.; Bill, E.; Dau, H.; Comba, P.; Ray, K. An Oxo Cobalt(IV) Complex Stabilized by Lewis Acid Interactions with Scandium(III)Ions. *Angew. Chem., Int. Ed.* **2011**, *50*, 1711–1715.

39 Prokop, K. A.; de Visser, S. P.; Goldberg, D. P. Unprecedented Rate Enhancements of Hydrogen-Atom Transfer to a Manganese(V)-Oxo Corrolazine Complex. *Angew. Chem., Int. Ed.* **2010**, *49*, 5091–5097.

40 Kumar, A.; Goldberg, I.; Botoshansky, M.; Buchman, Y.; Gross, Z. Oxygen Atom Transfer Reactions from Isolated (Oxo)Manganese(V) Corroles to Sulphides. *J. Am. Chem. Soc.* **2010**, *132*, 15233–15245.

41 (a) Danovich, D.; Shaik, S. Spin-Orbit Coupling in the Oxidative Activation of H-H by FeO^{+}. Selection Rules and Reactivity Effects. *J. Am. Chem. Soc.* **1997**, *119*, 1773–1786. (b) Shiota, Y.; Yoshizawa, K. A Spin-Orbit Coupling Study on the Spin Inversion Processes in the Direct Methane-to-Methanol Conversion by FeO^{+}. *J. Chem. Phys.* **2003**, *118*, 5872–5879.

42 (a) Poli, R.; Harvey, J. N. Spin Forbidden Chemical Reactions of Transition Metal Compounds. New Ideas and New Computational Challenges. *Chem. Soc. Rev.* **2003**, *32*, 1–8. (b) Manner, V. W.; Lindsay, A. D.; Mader, E. A.; Harvey, J. N.; Mayer, J. M. Spin-Forbidden Hydrogen Atom Transfer reaction in a Cobalt Biimidazoline System. *Chem. Sci.* **2012**, *3*, 230–243.

43 Bukowski, M. R.; Koehntop, K. D.; Stubna, A.; Bominaar, E. L.; Halfen, J. A.; Münck, E.; Nam, W.; Que, L., Jr. A Thiolate-Ligated Nonheme Oxoiron(IV) Complex Relevant to Cytochrome P450. *Science* **2005**, *310*, 1000–1002.

44 Mayer, J. M. Understanding Hydrogen Atom Transfer: From Bond Strength to Marcus Theory. *Acc. Chem. Res.* **2011**, *44*, 36–46.